Liquid Crystals
Publication details, including instructions for authors and subscription information:
http://www.informaworld.com/smpp/title~content=t713926090

Kossel diagrams of blue phases

B. Jérôme[a]; P. Pieranski[a]
[a] Laboratoire de Physique des Solides, Université de Paris-Sud, Orsay, Cedex, France

To cite this Article Jérôme, B. and Pieranski, P.(1989) 'Kossel diagrams of blue phases', Liquid Crystals, 5: 3, 799 — 812
To link to this Article: DOI: 10.1080/02678298908026386
URL: http://dx.doi.org/10.1080/02678298908026386

LIQUID CRYSTALS, 1989, VOL. 5, NO. 3, 799–812

Kossel diagrams of blue phases

by B. JÉRÔME and P. PIERANSKI
Laboratoire de Physique des Solides, Université de Paris-Sud, Bâtiment 510, 91405 Orsay Cedex, France

CB15/E9 mixtures submitted to an electric field exhibit a tetragonal phase BPX, having a $D_4^{10}(I4_122)$ symmetry and two hexagonal phases BPH^{3d} and BPH^{2d} The Kossel diagram technique allows us (*a*) to confirm the hexagonal symmetry of BPH^{3d} and to determine precisely its space group $D_6^2(P6_222)$ and (*b*) to study the field-induced phase transitions between BP II, BPX and BPH^{3d}. We show that the BP II → BPH^{3d} transition is a continuous deformation involving a dilatation in the field direction and a shear perpendicular to this direction. The BP II → BPX and BPX → BPH^{3d} transitions are discontinuous.

1. Introduction

Cholesteric liquid crystals with a sufficiently short pitch exhibit several blue phases at the transition between the cholesteric and isotropic phases. When no external field is applied, three different blue phases may occur in the phase diagram (T, K), where T is the temperature and K the chirality. BP I and BP II have respectively $O^8(I4_132)$ and $O^2(P4_232)$ symmetries, BP III is an amorphous phase. The behaviour of blue phases is modified by the presence of an electric field and depends on the sign of the dielectric anisotropy ($\varepsilon_a = \varepsilon_{\parallel} - \varepsilon_{\perp}$). In this paper we focus on mixtures of the cholesteric CB15 with the nematic E9 [1], which have a positive dielectric anisotropy. The case of compounds with negative ε_a is considered in a separate paper [2].

In an electric field, CB15/E9 mixtures with a concentration c of CB15, exhibit three other blue phases (see figure 1).

(*a*) BPX has a tetragonal symmetry $D_4^{10}(I4_122)$ and is oriented with the four-fold axis parallel to **E**. BPX crystals can be obtained by increasing **E** above a threshold field, either from BP I crystals oriented with the [110] axis parallel to **E** (c < 46 per cent) or from BP II crystals oriented with the [001] axis parallel to **E** (46 per cent < c < 33·53 per cent). The BP I → BPX transition is characterized by the sudden change of the crystals' shape, from a two- to a four-fold symmetry. The BP II → BPX transition is characterized by the discontinuous increase of the wavelength of the circularly polarized Bragg reflection $\lambda_{BP\,II}^{(001)}(E)$ [3].

(*b*) BPH^{3d} has a hexagonal symmetry and is oriented with the six-fold axis parallel to **E**. It appears either from BP II (53 per cent < c) or BPX (48 per cent < c < 53 per cent) by increasing the electric field above a threshold field. Both transitions are characterized by the change of the crystals' shape from a square to a hexagonal one; moreover, the BPX → BPH^{3d} transition induces a discontinuous decrease of the wavelength of the circularly polarized Bragg reflection $\lambda_{BPX}^{(002)}$ [3, 4].

0267-8292/89 $3.00

(*c*) BPH^{2d} also has a hexagonal symmetry and has the same orientation as BPH^{3d}. It occurs for higher fields than BPH^{3d} for 52 per cent < *c*. The $BPH^{3d} \rightarrow BPH^{2d}$ transition is characterized by the disappearance of the back reflection $\lambda^{(0001)}_{BPH^{3d}}$ [5].

The purpose of this paper is to use the Kossel diagram technique, already used to study the BP I → BPX transition [3] and to confirm the O^2 symmetry of BP II [6], in order to determine the space group of BPH^{3d} and to study the different observed transitions between the three phases BP II, BPX and BPH^{3d}. The experimental set-up is described in § 2. In § 3 we show the experimental Kossel diagrams of BPH^{3d} and discuss the possible symmetries of this phase. In § 4 we describe the field-induced phase transitions BP II → BPH^{3d}, BP II ↔ BPH^{3d}, BP II ↔ BPX and BPX ↔ BPH^{3d} between the phases occurring on the phase diagram (*E*, *c*) of figure 1.

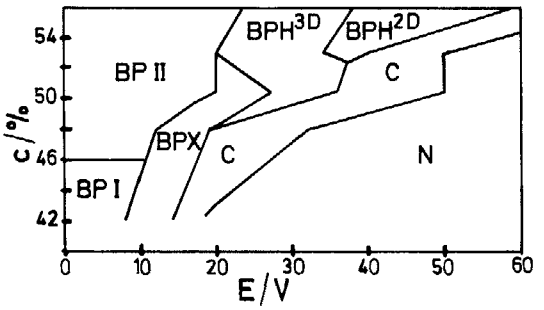

Figure 1. Phase diagram (*c*, *E*), where *c* is the weight concentration of CB15 in the mixture with E9 and *E* is the electric field applied to a 10 μm thick sample. The phases indicated are those appearing first when cooling the sample from the isotropic phase.

2. Experimental set-up

The experimental set-up is similar to that described in [2, 5]. The cell is shown in figure 2; the liquid crystal is located between a glass plate (GP) and a glass cylinder (GC). The glass plate is coated with a semitransparent InO electrode connected to the output E of an A.C. generator. The glass cylinder is coated with an evaporated aluminium film acting as a mirror and as an electrode connected to earth.

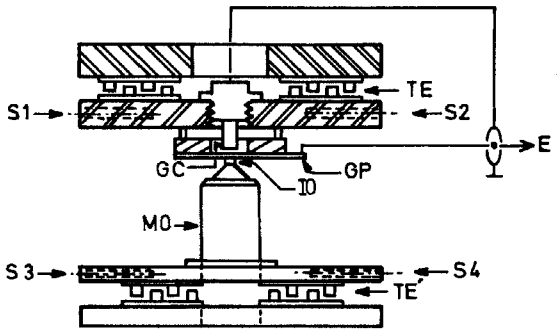

Figure 2. Experimental cell: GC, glass cylinder; TE and TE', thermoelectric elements; S1–S4 temperature probes; GP glass plate; IO, immersion oil; MO, microscopic objective; E, A.C. generator.

The light reflected by the mirror illuminates the background of the Kossel diagrams. In order to increase the contrast of the Kossel lines, we have obturated half of the incident light beam by introducing an opaque screen in the focal plane of the condenser; this screen suppresses one half of the beams to be reflected in the mirror and so darkens the background in one half of the Kossel diagrams (see figure 3). Note that the presence of the screen suppresses the superposition of two sets of Kossel lines S_1 and S_2 produced by the mirror [6]. This is important to enable a three- and a six-fold symmetry to be distinguished. As S_1 and S_2 are related by the inversion symmetry with respect to the centre of the focal plane, the superposition of S_1 and S_2 each having a three-fold symmetry, gives a diagram with a six-fold symmetry: without the screen the distinction between a three- and a six-fold symmetry is not possible.

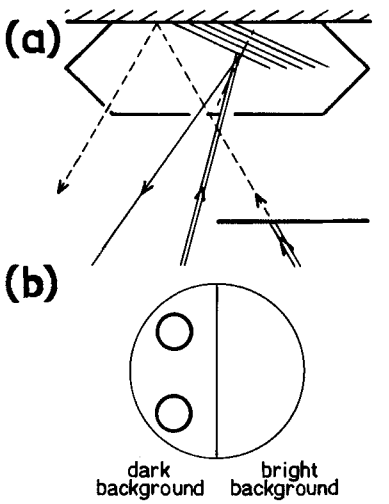

Figure 3. (*a*) Beam trajectories and (*b*) corresponding Kossel diagram; double line, incident beam; single line, reflected beam; broken line, beam suppressed by the screen.

3. The structure of BPH^{3d} from its Kossel diagrams

Figure 4 shows an experimental Kossel diagram of BPH^{3d} and the corresponding theoretical diagram (all of the theoretical diagrams are constructed with the same rules as in [3, 6]). This diagram confirms the three dimensional hexagonal symmetry of BPH^{3d}. The possible space groups compatible with this symmetry and with the absence of mirror planes in blue phases are listed in the table. All of these space groups allow $m = 2$ components [7] for the $(10\bar{1}0)$ and $(10\bar{1}1)$ lines; these are the indices of the two families of lines observed in the experimental Kossel diagram shown in figure 4. The behaviour of the (0001) line, indicated for each possible space group in the table, allows discrimination between the different possible space groups. The light reflected by the (0001) planes is circularly polarized and its intensity does not decrease to zero when the incidence becomes normal; this behaviour is characteristic of an $m = 2$ component. According to the table, the only possible space groups are $P6_2$ and $P6_222$ (or $P6_4$ and $P6_422$ according to the chirality of the compound). We show in § 4 that the study of the BP II $\rightarrow$ BPH^{3d} transition allows us to discard the first possibility.

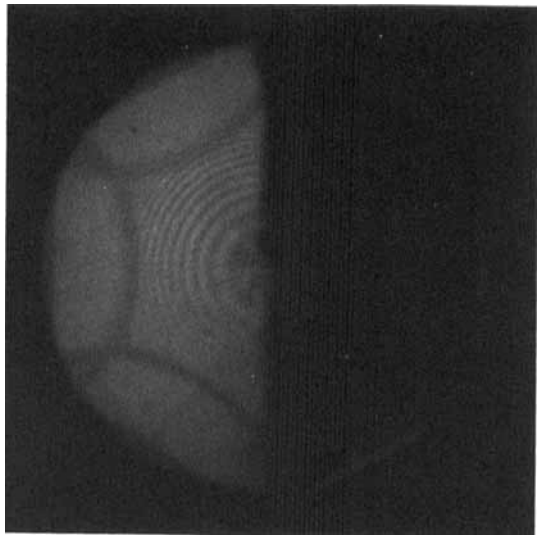

(*a*)

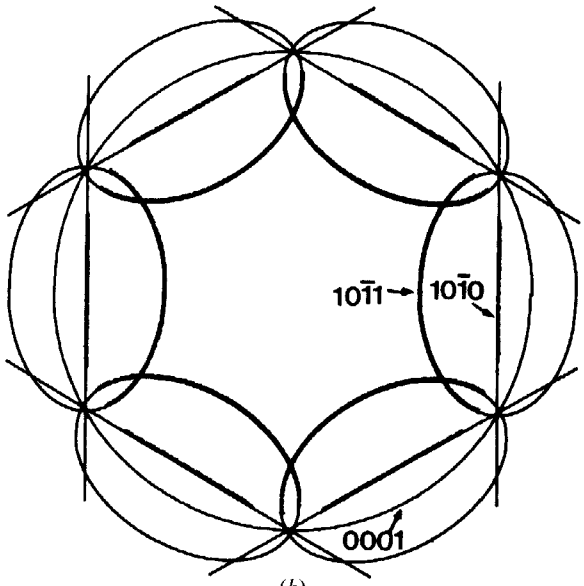

(*b*)

Figure 4. Kossel diagrams for BPH^{3d}: (*a*) CB15/E9 52·94 per cent, $\lambda = 380$ nm; (*b*) theory.

4. Field-induced phase transitions

4.1. *BP II → BPH^{3d} transition*

This transition occurs when an electric field is applied to a CB15/E9 mixture when the concentration c of CB15 is > 53 per cent.

4.1.1. *Kossel diagram observation*

When $E = 0$, BP II crystals oriented with their [001] axis parallel to **E** show the Kossel lines characteristic of their $O^2(P4_232)$ symmetry: the central $(001)_{II}$ ring, the

Possible space groups of BPH^{3d}. For each one we give the symmetry axes parallel to the [0001] axis of the crystal, the Fourier components of the (0001) and (0002) lines, and the expected behaviour of these lines.

Space group	Symmetry axes ∥ [0001]	Line indices	Fourier components $m=2$	$m=1$	$m=0$	Characteristic of the reflection
P6	6	(0001)			x	
	3	— —	— —	— —	— —	— — — — — —
P622	2	(0002)			x	
$P6_1(P6_5)$	6_1 (6_5)	(0001)		x		No intensity for normal incidence
	3_1 (3_2)	— —	— —	— —	— —	— — — — — —
$P6_122(P6_522)$	2_1 (2_1)	(0002)	x			Circularly polarized
$P6_2(P6_4)$	6_2 (6_4)	(0001)	x			Circularly polarized
	3_2 (3_1)	— —	— —	— —	— —	— — — — — —
$P6_222(P6_422)$	2 (2)	(0001)				
$P6_3$	6_3	(0001)				
	3	— —	— —	— —	— —	— — — — — —
$P6_322$	2_1	(0002)				

$(100)_{II}$ and the $(101)_{II}$ lines. When E is increased, BP II is distorted ($BP II_d$): the wavelength $\lambda_{BP II_d}^{(001)}$ at which the $(001)_{II_d}$ line appears, increases continuously [3]. At the threshold field $E_{II_d/H}$, the Kossel lines obtained for $BP II_d$ are replaced by those characteristic of BPH^{3d} (see figure 4(*a*)). The $(001)_{II_d}$ ring becomes the $(0001)_H$ ring without any change of the diameter (when $c < 56$ per cent).

The orientation of the diagrams obtained just before and just after the transition are related (see figure 5): one pair of opposite wavevectors equivalent to $[10\bar{1}0]_H$ in BPH^{3d} (for example, $[10\bar{1}0]_H$ and $[\bar{1}010]_H$) is parallel to one pair of opposite wavevectors equivalent to $[100]_H$ in $BP II_d$ (for example, $[100]_{II_d}$ and $[\bar{1}00]_{II_d}$). Thus, there are two possible orientations of the BPH^{3d} diagram with respect to that of $BP II_d$ ($[10\bar{1}0]_H \parallel [100]_{II_d}$ or $[010]_{II_d}$). Note that in the reverse transition $BPH^{3d} \rightarrow BP II_d$ there are three possible orientations of the $BP II_d$ diagram with respect to that of BPH^{3d} ($[100]_{II_d} \parallel [10\bar{1}0]_H$, $[01\bar{1}0]_H$ or $[1\bar{1}00]_H$). This relationship between orientations of Kossel diagrams is the same as that deduced from observation of crystal shapes in [5].

4.1.2. *Deformation of the BP II lattice in real space*

BP II has a simple cubic $O^2(P4_232)$ symmetry. The basis vectors of the simple cubic lattice are

$$\mathbf{x}_1^{II} = a\mathbf{i}, \qquad \mathbf{x}_2^{II} = a\mathbf{j}, \qquad \mathbf{z}^{II} = a\mathbf{k},$$

with $\mathbf{i}$, $\mathbf{j}$, $\mathbf{k}$ three unit vectors parallel to the edges of the cell. When the electric field is increased from zero the lattice parameter along the [001] axis increases:

$$\mathbf{x}_1^{II_d} = \frac{1}{[\varepsilon_1(E)]^{1/2}} a\mathbf{i}, \qquad \mathbf{x}_2^{II_d} = \frac{1}{[\varepsilon_1(E)]^{1/2}} a\mathbf{j}, \qquad \mathbf{z}^{II_d} = \varepsilon_1(E) a\mathbf{k},$$

(we have assumed that the crystal is incompressible) with

$$\varepsilon_1(0) = 1, \qquad \frac{d\varepsilon_1}{dE} > 0.$$

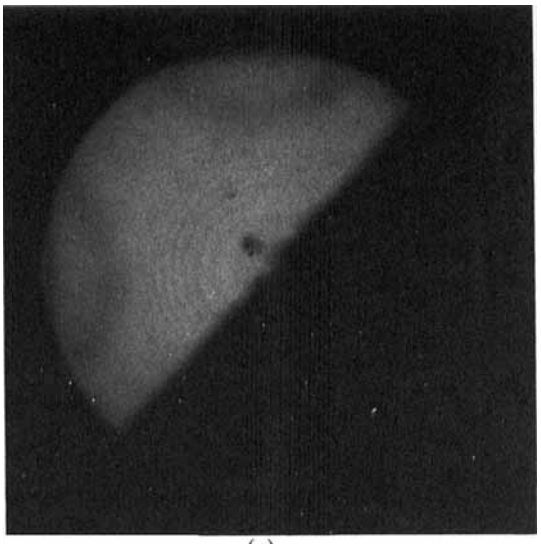

(*a*)

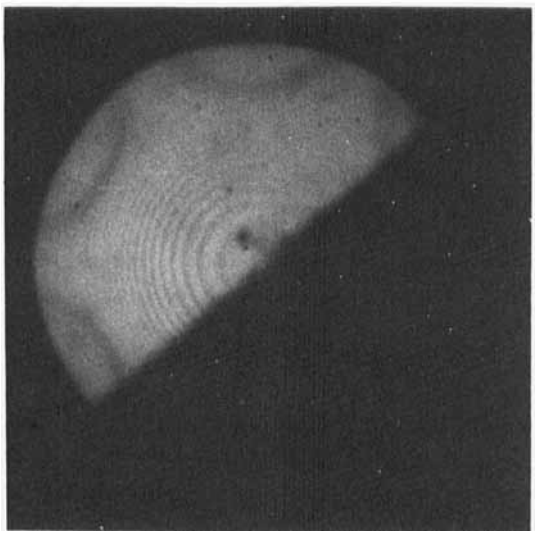

(*b*)

Figure 5. Kossel diagram for CB15/E9 52·94 per cent, $\lambda = 400\,\text{nm}$: (*a*) BP II_d, $E = E^{-}_{\text{II}_\text{d}/\text{H}}$; (*b*) $\text{BPH}^{3\text{d}}$, $E = E^{+}_{\text{II}_\text{d}/\text{H}}$; (*c*) and (*d*) corresponding theoretical diagrams.

The symmetry of the resulting lattice, shown in figure 6(*a*), is simple tetragonal $D_4^5(P4_222)$.

At $E = E_{\text{II}_\text{d}/\text{H}^{3\text{d}}}$ the crystal undergoes a shear in the plane perpendicular to **E**, the lattice parameter along the [001] axis remaining constant:

$$\mathbf{x}_1^i = \frac{1}{(\sin\alpha)^{1/2}} \frac{1}{\beta_1^{1/2}} a\,(\sin\alpha\,\mathbf{i} - \cos\alpha\,\mathbf{j}),$$

$$\mathbf{x}_2^i = \frac{1}{(\sin\alpha)^{1/2}} \frac{1}{\beta_1^{1/2}} a\mathbf{j},$$

$$\mathbf{z}^i = \beta_1 a\mathbf{k},$$

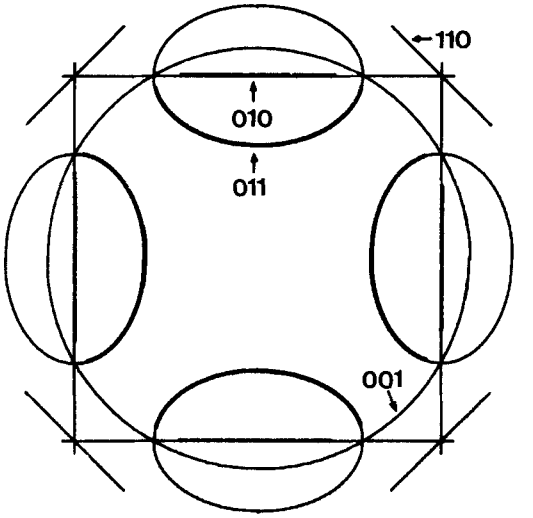

(*c*)

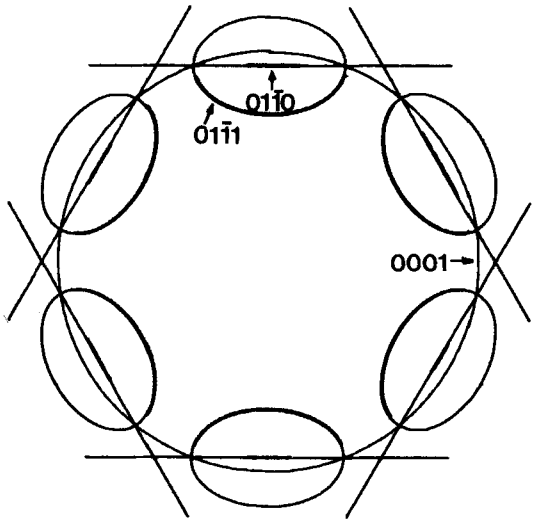

(*d*)

Figure 5. *Continued.*

with

$$\beta_1 = \varepsilon_1(E_{\mathrm{II_d/H^{3d}}}).$$

The symmetry of this intermediate lattice is C-centred orthorhombic D_2^6(C222). During the transition, α varies from $\pi/2$ in BP II to $\pi/3$ in PBH^{3d}; for this phase, the basis vectors of the hexagonal lattice, shown in figure 6(*b*), are

$$\mathbf{x}_1^{\mathrm{H}} = \left(\frac{2}{3^{1/2}}\right)^{1/2} \frac{1}{\beta_1^{1/2}} a \left(\frac{3^{1/2}}{2}\mathbf{i} - \frac{1}{2}\mathbf{j}\right),$$

$$\mathbf{x}_2^{\mathrm{H}} = \left(\frac{2}{3^{1/2}}\right)^{1/2} \frac{1}{\beta_1^{1/2}} a\mathbf{j},$$

$$\mathbf{z}^{\mathrm{H}} = \beta_1 a\mathbf{k}.$$

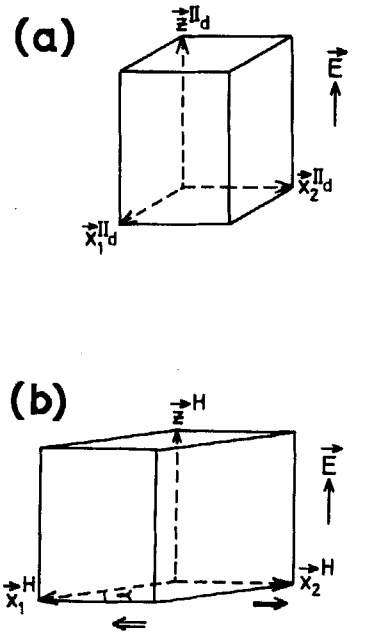

Figure 6. (*a*) BP II_d and (*b*) BPH^{3d} real lattice.

The only possible space groups for BPH^{3d} are those which give a $D_2^6(C222)$ symmetry when submitted to a shear reverse to that considered here, i.e. an increase of α from $\pi/3$; these space groups are P622 and $P6_222$ (or $P6_422$). The first is incompatible with the behaviour of the experimentally observed (0001) Kossel line (see § 3), so we conclude that the symmetry of BPH^{3d} is $D_6^4(P6_222)$. This is in agreement with the theoretical results of Hornreich and Shtrikman showing the existence of a phase with a D_6^4 symmetry in the (T, E) phase diagram [8].

4.1.3. *Deformation of BP II lattice in reciprocal space*

The basis vectors of the reciprocal simple cubic lattice of BP II are

$$\mathbf{a}_1^{II} = (2\pi/a)\mathbf{i}, \qquad \mathbf{a}_2^{II} = (2\pi/a)\mathbf{j}, \qquad \mathbf{c}^{II} = (2\pi/a)\mathbf{k}.$$

In a non-zero field, this lattice is transformed into the simple tetragonal lattice shown in figure 7 (*a*), with basis vectors given by

$$\mathbf{a}_1^{II_d} = [\varepsilon_1(E)]^{1/2}(2\pi/a)\mathbf{i},$$

$$\mathbf{a}_2^{II_d} = [\varepsilon_1(E)]^{1/2}(2\pi/a)\mathbf{j},$$

$$\mathbf{c}^{II_d} = [1/\varepsilon_1(E)](2\pi/a)\mathbf{k}.$$

During the BP $II_d \rightarrow BPH^{3d}$ transition, this lattice undergoes the reciprocal shear to the shear parallel to $\mathbf{x}_2^{II_d}$ considered in § 4.1.3, i.e. a shear parallel to $\mathbf{a}_1^{II_d}$. The basis

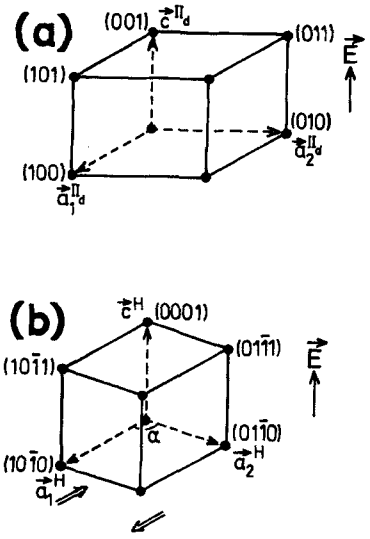

Figure 7. (*a*) BP II_d and (*b*) BPH^{3d} reciprocal lattice.

vectors of the resulting lattice, shown in figure 7 (*b*) are

$$\mathbf{a}_1^H = \left(\frac{2}{3^{1/2}}\right)^{1/2} \beta_1^{1/2}(2\pi/a)\mathbf{i},$$

$$\mathbf{a}_2^H = \left(\frac{2}{3^{1/2}}\right)^{1/2} \beta_1^{1/2} \frac{2\pi}{a}\left(\frac{1}{2}\mathbf{i} + \frac{3^{1/2}}{2}\mathbf{j}\right),$$

$$\mathbf{c}^H = \frac{1}{\beta_1}\frac{2\pi}{a}\mathbf{k}.$$

With such a transition the $[10\bar{1}0]_H$ axis of the resultant BPH^{3d} lattice is parallel to the $[100]_{II_d}$ axis of the initial BP II_d lattice; the other possible orientation of the BPH^{3d} lattice with respect to the BP II_d lattice is obtained by considering in reciprocal space, a shear parallel to $\mathbf{a}_2^{II_d}$ instead of $\mathbf{a}_1^{II_d}$. In the reverse transition the three possible orientations of the BP II_d lattice with respect to that of BPH^{3d} are obtained by considering, in reciprocal space, shears parallel to $\mathbf{a}_1^H$, $\mathbf{a}_2^H$ or $\mathbf{a}_1^H - \mathbf{a}_2^H$. These orientation relationships are in agreement with the experimentally observed relative orientations of BPH^{3d} and BP II_d crystal facets and Kossel diagrams (see §4.1.1).

4.2. *BP II → BPX transition*

When the concentration of CB15 in the CB15/E9 mixture is 46 per cent $< c <$ 53 per cent, BP II is transformed into BPX by applying an electric field greater than the threshold $E_{II_d/X}$.

4.2.1. *Kossel diagram observation*

The evolution of BP II into BP II_d when the field is increased is the same as for the BP II → BPH^{3d} transition. Figure 8 (*a*) shows the $(100)_{II_d}$ and $(101)_{II_d}$ lines of BP II_d just before the transition into BPX. This transition is characterized by the appearance

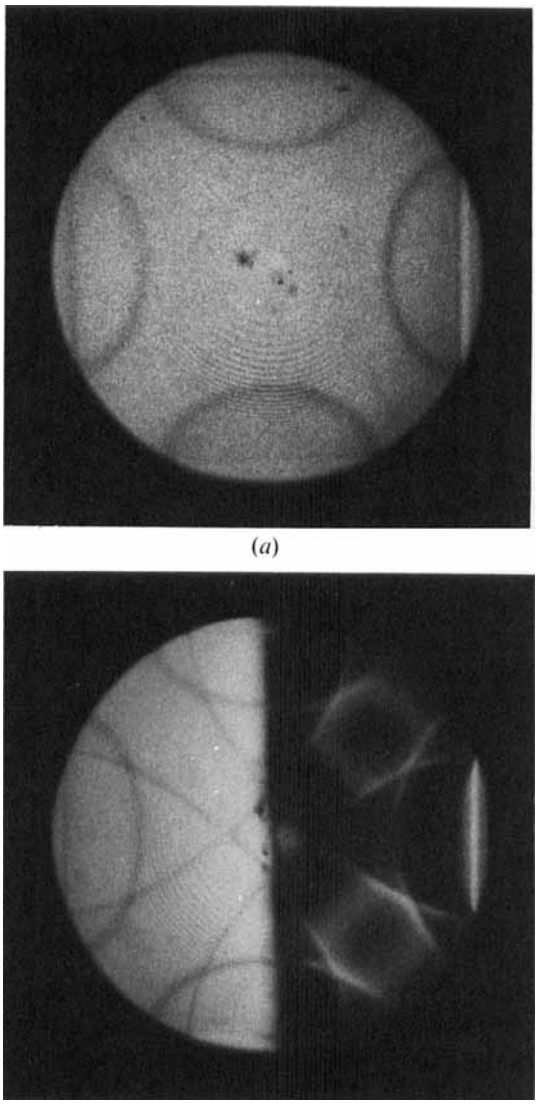

Figure 8. Kossel diagrams for CB15/E9 48·05 per cent, $\lambda = 436$ nm: (*a*) BP II$_d$, $E = E^{-}_{II_d/X}$; (*b*) BPX, $E = E^{+}_{II_d/X}$; (*c*) and (*d*) corresponding theoretical diagrams.

of two additional families of lines (see figure 8 (*b*)): $(111)_X$ and $(113)_X$. The $(100)_{II_d}$ and $(101)_{II_d}$ lines become the $(200)_X$ and $(202)_X$ lines; the $(001)_{II_d}$ ring is replaced by the $(002)_X$ ring, which has a greater diameter because of the discontinuous increase of $\lambda^{(001)}_{BP\,II_d}$ into $\lambda^{(002)}_{BPX}$.

4.2.2. *Deformation of the BP II lattice in reciprocal space*

Just before the transition into BPX, the reciprocal lattice is the simple tetragonal lattice described in §4.1.3. At $E = E_{II_d/X}$ the lattice undergoes a sudden transition; (1) the lattice parameter along the direction parallel to **E** decreases, and (2) a node

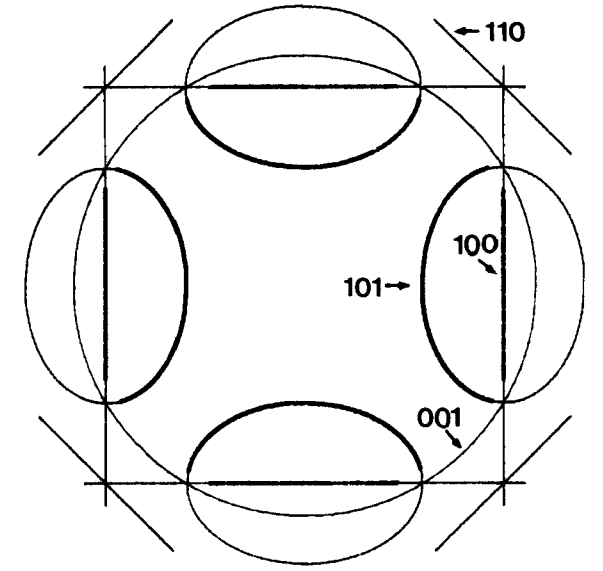

(*c*)

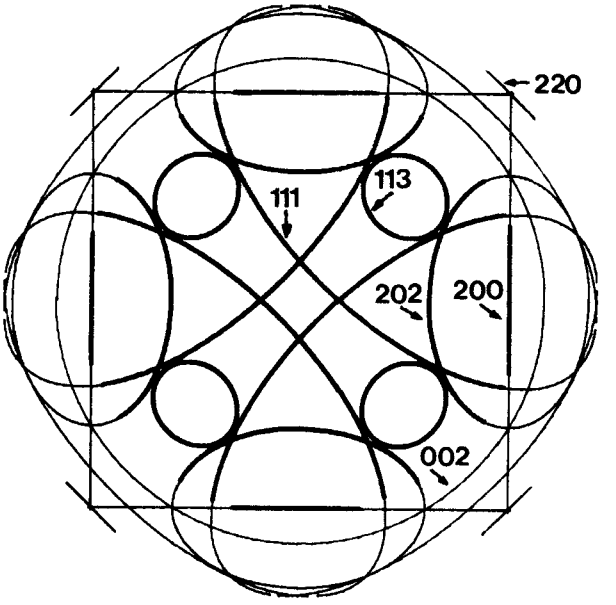

(*d*)

Figure 8. *Continued.*

appears in the centre of the tetragonal cell. The resultant centred tetragonal lattice is shown in figure 9; its basis vectors are

$$\mathbf{a}_1^x = \tfrac{1}{2}\beta_2^{1/2}\frac{2\pi}{a}\mathbf{i}, \qquad \mathbf{a}_2^x = \tfrac{1}{2}\beta_2^{1/2}\frac{2\pi}{a}\mathbf{j}, \qquad \mathbf{c}^x = \frac{1}{2}\frac{1}{\beta_2}\frac{2\pi}{a}\mathbf{k},$$

with

$$\beta_2 = \varepsilon_2\varepsilon_1 E_{\mathrm{II}_d/X}, \qquad \varepsilon_2 > 1.$$

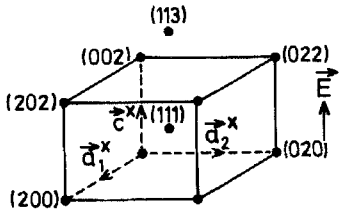

Figure 9. BPX reciprocal lattice.

4.2.3. *Deformation of the BP II lattice in real space*

The basis vectors of the BPX real lattice can be deduced from those of the reciprocal lattice:

$$\mathbf{x}_1^x = 2\frac{1}{\beta_2^{1/2}}a\mathbf{i}, \qquad \mathbf{x}_2^x = 2\frac{1}{\beta_2^{1/2}}a\mathbf{j}, \qquad \mathbf{z}^x = 2\beta_2 a\mathbf{k}.$$

They define the edges of a face-centred tetragonal cell containing four simple tetragonal cells of the BP II_d lattice. With a change of the basis vectors ($\mathbf{x}_1^x$, $\mathbf{x}_2^x$, $\mathbf{z}^x$) by

$$\mathbf{x}_1'^x = 2\frac{1}{\beta_2^{1/2}}a(\mathbf{i} + \mathbf{j}),$$

$$\mathbf{x}_2'^x = 2\frac{1}{\beta_2^{1/2}}a(-\mathbf{i} + \mathbf{j}),$$

$$\mathbf{z}'^x = \mathbf{z}^x,$$

we obtain the conventional body-centred tetragonal cell the $D_4^{10}(I4_122)$ lattice.

The BP II → BPX transition can also be described in terms of the representation of blue phases by a network of disclinations [9]. In the case of BP II this network is composed of two identical interwoven diamond lattices. When an electric field is applied, these two lattices deform in the same manner and remain identical; the symmetry is $P4_222$. At the BP II_d → BPX transition the two lattices differentiate themselves; the symmetry becomes $I4_122$.

4.3. *BPX → BPH^{3d} transition*

This transition occurs in CB15/E9 mixtures with 48 per cent < c < 53 per cent.

4.3.1. *Kossel diagram observation*

At the transition, the Kossel lines obtained for BPX (see figure 8 (*b*)) are replaced by those characteristics of BPH^{3d} (see figure 4 (*a*)). There is the same relationship between BPH^{3d} and BPX orientations as between BPH^{3d} and BP II orientations in the BP II → BPH^{3d} transition (see § 4.3.1). The $(002)_X$ ring is replaced by the $(001)_H$ ring which has a smaller diameter because of the discontinuous decrease of $\lambda_{BPX}^{(002)}$ into $\lambda_{BPH^{3d}}^{(0001)}$.

4.3.2. *Deformation of the BPX lattice in reciprocal space*

The deformation of the body-centred tetragonal reciprocal lattice of BPX at BPX → BPH^{3d} transition occurs in the following way: (1) the lattice parameter along the direction parallel to **E** increases; (2) the node located in the centre of the tetragonal

cell disappears; and (3) the lattice undergoes a shear identical to that undergone by the BP II_d reciprocal lattice during the BP $II_d \rightarrow BPH^{3d}$ transition (see §4.1.3). The resultant lattice is the same as that resulting from the BP II $\rightarrow BPH^{3d}$ transition.

4.3.3. *Deformation of the BPX lattice in real space*

The deformation of the face-centred tetragonal lattice of BPX (obtained from the conventional body-centred tetragonal lattice by a change of basis vectors) at the BPX $\rightarrow BPH^{3d}$ transition can be deduced from the deformation of the reciprocal lattice: (1) the lattice parameter along the direction parallel to the **E** decreases; (2) the face-centred tetragonal cell is divided into four identical simple tetragonal cells; and (3) the lattice undergoes a shear identical to that undergone by the BP II_d real lattice during the BP $II_d \rightarrow BPH^{3d}$ transition (see §4.1.2). The resultant lattice has the same symmetry as that obtained by the BP II $\rightarrow BPH^{3d}$ transition, i.e. $D_6^4(P6_222)$.

5. Conclusion

We have studied the Kossel diagrams of three different blue phases exhibited by CB15/E9 mixtures subjected to an electric field: BP II, BPX and BPH^{3d}. By means of the observation of BPH^{3d} Kossel diagrams, we have been able to confirm the three dimensional hexagonal symmetry of BPH^{3d} and to determine precisely its space group, which is found to be $D_6^4(P6_222)$. The Kossel diagrams of the same blue phase crystal obtained just before and just after a phase transition have allowed us to determine the nature of the three observed transitions between BP II, BPX and BPH^{3d}:

(*a*) The BP II $\rightarrow BPH^{3d}$ transition consists of a continuous deformation of the $O^2(P4_232)$ lattice of BP II into the $D_6^4(P6_222)$ lattice of BPH^{3d} and can be summarized by the following sequence of symmetries:

$$\underset{\text{BP II}}{O^2(P4_232)} \xrightarrow{E\neq 0} \underset{\text{BP II}_d}{D_4^5(P4_222)} \xrightarrow{E=E_{II_d/H}^-} D_2^6(C222) \xrightarrow{E=E_{II_d/H}^+} \underset{BPH^{3d}}{D_6^4(P6_222)}$$

The deformation can be seen as an elongation in the field direction, transforming the cubic O^2 lattice into the tetragonal D_4^5 lattice, followed by a shear perpendicular to the field direction which transforms the D_4^5 lattice into the orthorhombic (D_4^6) and, finally, the hexagonal (D_6^4).

(*b*) The BP II $\rightarrow$ BPX transition decomposes itself in the following stages:

$$\underset{\text{BP II}}{O^2(P4_232)} \xrightarrow{E\neq 0} \underset{\text{BP II}_d}{D_4^5(P4_222)} \xRightarrow{E=E_{II_d/X}} \underset{BPX}{D_4^{10}(I4_122)}$$

The first is the same continuous deformation as in the BP II $\rightarrow BPH^{3d}$ transition. The second is a discontinuous symmetry change.

(*c*) The BPX $\rightarrow BPH^{3d}$ transition is discontinuous:

$$\underset{BPX}{D_4^{10}(I4_122)} \xRightarrow{E=E_{X/H}} \underset{BPH^{3d}}{D_6^4(P6_222)}$$

This transition includes a discontinuous change of symmetry, a compression in the field direction and a shear perpendicular to this direction. All of these transformations occur together and no intermediate symmetry can be defined.

We thank B. Pansu for illuminating discussions about the space group symmetries.

References

[1] CB15 and E9 are produced by B.H.D. Chemicals.
[2] HEPPKE, G., JÉRÔME, B., KITZEROW, H.-S., and PIERANSKI, P., 1989, *Liq. Crystals*, **5**, 813.
[3] CLADIS, P. E., GAREL, T., and PIERANSKI, P., 1986, *Phys. Rev. Lett.*, **57**, 2841. PIERANSKI, P., and CLADIS, P. E., 1987, *Phys. Rev.* A, **35**, 355.
[4] PIERANSKI, P., CLADIS, P. E., and BARBET-MASSIN, R., 1985, *J. Phys. Paris, Lett.*, **46**, L973.
[5] JORAND, M., and PIERANSKI, P., 1987, *J. Phys., Paris*, **48**, 1197.
[6] JÉRÔME, B., PIERANSKI, P., GODEC, V., HARAN, G., and GERMAIN, C., 1988, *J. Phys., Paris*, **49**, 837.
[7] GREBEL, H., HORNREICH, R. M., and SHTRIKMAN, S., 1983, *Phys. Rev.* A, **28**, 1114.
[8] HORNREICH, R., and SHTRIKMAN, S. (preprint).
[9] MEIBOOM, S., SAMMON, M., and BRINKMAN, W. F., 1983, *Phys. Rev.* A, **27**, 438.